ACS Catalysis

Research Article

pubs.acs.org/acscatalysis

High Efficiency Cu-ZnO Hydrogenation Catalyst: The Tailoring of Cu-ZnO Interface Sites by Molecular Layer Deposition

Bin Zhang,[†] Yao Chen,[†] Jianwei Li,[†] Eckhard Pippel,[‡] Huimin Yang,[†] Zhe Gao,[†] and Yong Qin*[,†]

[†]State Key Laboratory of Coal Conversion, Institute of Coal Chemistry, Chinese Academy of Sciences, Taiyuan 030001, P.R. China

[‡]Max Planck Institute for Microstructure Physics, Weinberg 2, D-06120 Halle, Germany

Supporting Information

ABSTRACT: This paper describes a molecular layer deposition (MLD)-assisted route for the preparation of Cu-ZnO catalysts used in the hydrogenation of levulinic acid to produce γ-valerolactone. A Cu precursor supported on multiwalled carbon nanotubes was coated with Zn-polyurea organic–inorganic hybrid films via MLD first, and the catalyst was obtained after calcination and reduction under mild conditions. The produced catalysts exhibited remarkably enhanced selectivity, efficiency, and stability due to the created Cu-ZnO interface sites (Cu^0Zn) and the cooperative effect between Cu^0Zn and Cu^+. The ratio of Cu^0Zn sites could be simply modified by changing the MLD cycle number. The correlation between catalytic activity and the ratio of different Cu species (Cu^0Zn, Cu^0, and Cu^+) suggests that Cu^0Zn is the main active site and responsible for the remarkably enhancing catalytic activity and low apparent activation energy.

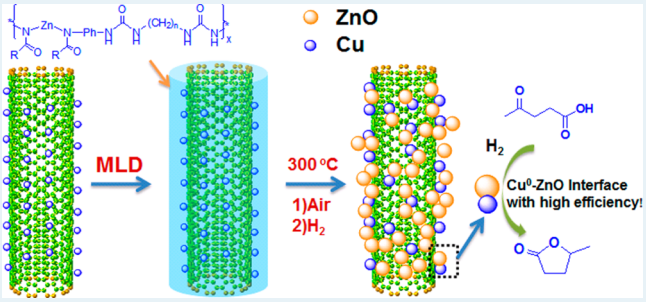

KEYWORDS: *molecular layer deposition, Zn-organic–inorganic hybrid film, Cu–ZnO interface, hydrogenation, nanoparticles, nanocatalysts*

1. INTRODUCTION

Hydrogenation of C═O bond, such as CO, CO_2, furfural and levulinic acid (LA), has emerged as a powerful way to produce a variety of chemicals and fuels from biomass, coal, and petroleum.[1−4] Copper-based catalysts are widely used for the hydrogenation of C═O bond due to their selectivity in hydrogenation of C═O bonds and inactivity for the hydrogenolysis of C−C bonds.[3,5,6] As the relatively unstable copper nanoparticles (NPs) tend to agglomerate or leach during preparation stages (or high temperature reactions), it is of vital importance to enhance their thermal and chemical stability without impairing their intrinsic high performance.[5,7] High-efficiency copper catalysts could be achieved mainly by tailoring the interplay of the metal-oxides and optimizing the microstructure by using special oxides as additive[5,8−10] or forming stable copper precursors.[3,7,11]

Cu-ZnO composites have wide applications in catalytic conversion of CO_2 or CO to methanol,[4,12−16] hydrogenation/dehydroxylation of biomass (fructose, sorbitol, glycerol or furfural) to diols,[6] photocatalytic H_2 production,[17] methanol steam reforming,[18] and gas sensors.[19] However, there is still a lack of understanding of the influence of Cu-ZnO interface on their activity and selectivity in the hydrogenation of carbonyl compounds, such as furfural and LA. In general, ZnO is widely used as an additive to improve the performance of Cu-ZnO methanol synthesis catalysts by two ways. First, ZnO NPs function as a physical spacer between Cu NPs and help to disperse the Cu phase during catalyst preparation, resulting in high copper surface area.[12,13] Second, the interaction of Cu and ZnO also leads to an increase of intrinsic activity of Cu-based methanol synthesis catalysts, an effect known as the Cu-ZnO synergy.[4,14−16] Behrens and co-workers have demonstrated that the Cu-ZnO synergy is related to the presence of $Zn^{\delta+}$ at the defective (stepped) Cu surface, which is a result of a strong Cu-ZnO interaction leading to a partial coverage of the Cu surface with ZnO_x under reducing conditions.[4] Substitution of Zn into the Cu steps further strengthens the binding of the intermediates and increases the catalytic activity. Liao and co-workers ascribed the synergy of Cu and ZnO in methanol production from CO_2 hydrogenation to certain interaction between ZnO and Cu NPs over the catalyst prepared by physically mixing Cu and ZnO NPs.[15] Recently, Valant and co-workers have discovered that the activity of the Cu-ZnO methanol synthesis catalyst is correlated to the number of contact points between Cu and ZnO NPs.[16] Therefore, it is crucial to tailor the interplay of Cu-ZnO interface for a high efficiency C═O hydrogenation catalyst. However, it is difficult to tailor the Cu-ZnO interface by traditional methods.

Atomic layer deposition (ALD) and molecular layer deposition (MLD) have shown to be effective in the generation of metal-oxide interface sites by overcoating the metal NPs with porous oxide films. ALD produces films by self-limiting chemical reactions between gaseous precursors and a solid surface in an

Received: February 21, 2015
Revised: August 5, 2015
Published: August 17, 2015

DOI: 10.1021/acscatal.5b01266
ACS Catal. 2015, 5, 5567−5573

atomic layer-by-layer fashion.[20] It was employed to engineer the metal-oxide interface in the subnanometer precision by coating the surface of metal NPs with oxide films.[21,22] In order to produce more metal-oxide interface sites on the surface of catalyst, high annealing temperature (>700 °C) is necessary to create microporsity in the ALD oxide films. MLD is a subset of ALD which produces polymer or organic−inorganic hybrid films using organic precursors by similar self-limiting surface reactions.[20,23−25] The obtained organic−inorganic hybrid films can be converted into porous oxide films after removing organic parts at lower temperature in comparison with ALD.[26,27] Besides, the porous structure of the film could be modified by the chemical structure of the organic part. Although metal NPs with a porous oxide shell can retain the catalytic activity and only sinter at much higher temperature, the porous shell still results in the loss of surface active sites and the annealing temperature is too high to generate porous shell.[27,28]

Herein, we demonstrate a new approach to tailor the Cu-ZnO interface by MLD. The Cu-ZnO catalysts are prepared by depositing a Zn-polyurea hybrid layer by MLD on the surface of Cu precursors supported on multiwalled carbon nanotubes (CNTs) and then calcinating at mild temperature. The low annealing temperature (300 °C) can prevent the aggregation of the produced CuO NPs. The use of polyuria as organic part of the Zn MLD film is beneficial to tailor Cu-ZnO interface sites by changing MLD cycle number. The activity and stability of the Cu catalyst for levulinic acid (LA) hydrogenation are significantly improved due to the generation of abundant Cu-ZnO interface sites.

2. EXPERIMENTAL SECTION

Precursors and Materials. Diethyl zinc ($Zn(Et)_2$, 1.0 M solution in hexanes) was obtained from J&K Scientific Ltd. It has a high vapor pressure and high reactivity and is wildly used as Zn source in ALD process.[20] The solution was injected into a precursor cylinder in a N_2 glovebox (O_2, H_2O < 1 ppm). 1,4-Phenylene diisocyanate (PPDI) and ethanediamine (EDA) were used without further purification. High purity N_2 (99.999%) was used as the purge gas and carrier gas. Urea and copper nitrate were used for the synthesis of copper precursors. CNTs were purchased from Shenzhen Nanotech Port Co. Ltd. (40−60 nm in diameter, 5−15 μm in length). CNTs were pretreated in concentrated nitric acid at 120 °C for 6 h before catalyst preparation. Commercial Cu−Zn−Al catalyst (MWC-612) was purchased from Lanzhou Katie Chemical Technology Co., Ltd.

Catalyst Preparation. First, 0.150 g treated CNTs were added into an aqueous solution of urea (0.148 g) and copper nitraties (0.152 g) at room temperature. Then, the reaction slurry was heated in an oil bath at 170 °C for 0.5 h. The resulting powders were dried at 110 °C overnight to obtain Cu/CNTs precursors. The MLD process was carried out in a hot-wall, closed chamber-type ALD reactor at 100 °C. Prior to MLD, 50 mg Cu/CNTs precursors dispersed in ethanol were spread out on a quartz wafer and dried in air. Then, Zn-hybrid films were deposited by sequential exposure of the Cu/CNTs precursors to $Zn(Et)_2$, PPDI, EDA and PPDI with x cycles (x is the MLD cycle number). Exposure and purge times for all precursors were 10 and 25 s, respectively. The temperature of the PPDI source was kept at 80 °C. After MLD process, the samples were transferred to a tube furnace and calcinated at 300 °C in air for 2 h producing Cu−Zn(x)MLD. For comparison, direct coating of ZnO on the Cu precursors by ALD was also performed by sequentially exposing the Cu/CNTs precursors to $Zn(Et)_2$ and H_2O with y cycles. Then the samples were calcinated at 300 °C in air to form Cu−Zn(y)ALD. Cu/CNTs precursors were also calcinated at 300 °C before the catalytic test to reveal the function of ZnO. It can be known by inductively coupled plasma optical emission spectroscopy (ICP-OES) that the contents of Cu in Cu−Zn-MLD and Cu/CNTs catalysts are around 20 and 25 wt %, respectively.

Catalytic Reaction. The performance evaluation of these catalysts was carried out in a tubular fixed-bed microreactor combined with an online gas chromatogram (GC). Prior to reaction, the catalyst was reduced in situ in a 10% H_2/N_2 (v/v) gas mixture under atmospheric pressure at 300 °C for 1 h, with a ramp of 2 K/min. Then 2 wt % solution of LA in ethanol was pumped into a vaporizer, mixed with carrier gas (40 mL/min N_2 and 20 mL/min H_2) and then introduced into the reactor. The total pressure in the reactor was kept at 1.0 MPa. The reaction products were analyzed using GC(GC-9720, Zhejiang Fuli chromatogram analysis Co., Ltd., China) equipped with a hydrogen flame ionization detector (FID) and a capillary column (HP-5, 30 m × 0.32 mm). The conversion and selectivity were determined based on the area normalization method.

Characterization and Equipment. TEM and high-resolution TEM (HRTEM) images were collected using a JEOL JEM 2100F instrument. The concentration of the metal in the catalyst was determined by ICP-OES, (Thermo iCAP 6300, U.S.A.). Fourier-transform infrared (FTIR) spectroscopy measurements were performed on a Bruker VEREX70 (Germany) using a MCT-A detector in the transmission mode. Spectra were taken with 60 scans at 4 cm^{-1} resolution. The MLD films were deposited onto a KBr pellet for FTIR analysis. XRD analysis was carried out on a D/max-RA X-ray diffractometer (Rigaku, Japan) with Cu Kα radiation (λ = 0.154 nm) operated at 40 kV. The Cu crystallite size was calculated with the Scherrer equation using the full width at half-maximum (fwhm) of the Cu(111) diffraction peak at 2θ = 43.2°. Thermogravimetric (TG) was performed on Rigaku TG analyzer at a 10 K/min scan rate in air from 30 to 800 °C. X-ray photoelectron spectroscopy (XPS) and auger electron spectroscopy (AES) were recorded with a VG MiltiLab 2000 system at a base pressure of 1×10^{-9} mbar. Samples were excited with monochromatized Mg Kα radiation ($h\nu$ = 1253.6 eV). The analyzer was operated in a constant-pass energy mode (20 eV). In order to reveal the real surface structure of the catalysts in the hydrogenation process, Cu catalysts were reduced in 10% H_2/N_2 gas mixture at 300 °C for 1 h in the XPS pretreatment chamber prior to XPS measurement. The exposed copper surface area was measured using N_2O chemisorption method as described previously (Cu surface atom density: 1.47×10^{19} atoms/m^2).[29−32]

3. RESULTS AND DISCUSSION

Scheme 1 shows the proposed reaction sequence for the four-step (ABCB) MLD process of the Zn-hybrid film growth. First, PPDI (B) is noncovalently adhered onto the surface of samples (MWCNTs or copper precursors) via strong physical adsorption.[33] Second, the reaction of $Zn(Et)_2$ (A) with adsorbed PPDI (B) molecules proceeds by the insertion of one isocyanate group (-NCO) into the Zn-Et bond, giving the half heteroleptic amidate complex.[34] Then PPDI molecules are introduced and react with surface -Zn-Et to form complete heteroleptic amidate complex. Other −NCO groups can then react with EDA (C) molecules in the following step to form a $-NHCH_2CH_2NH_2$ terminated surface, which can anchor PPDI (B) molecules to leave −NCO groups in the final step.[35] This four-step ABCD

DOI: 10.1021/acscatal.5b01266
ACS Catal. 2015, 5, 5567−5573

Scheme 1. Proposed Four-Step (ABCB) Reaction Sequence for Zn-Hybrid Film Formation by MLD using $Zn(Et)_2$, PPDI, and EDA as Precursors

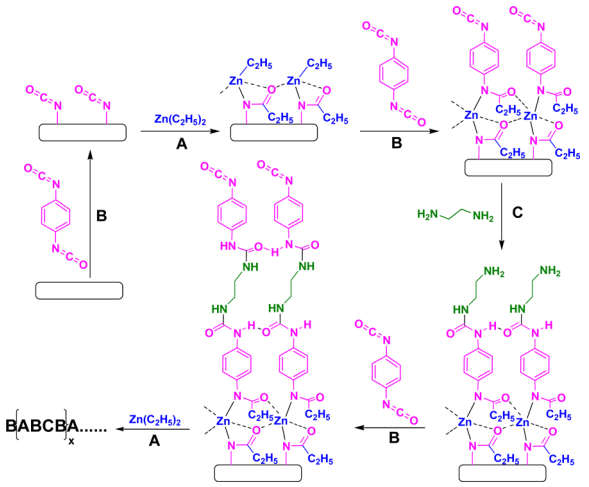

sequence is repeated until the required Zn hybrid film thickness is obtained. The process enables tuning of the distance between adjacent Zn moieties through the length of the organic part.[36]

The FTIR spectra (Figure 1) and XPS results (Supporting Information, Figure S3) confirm the successful covalent bonding

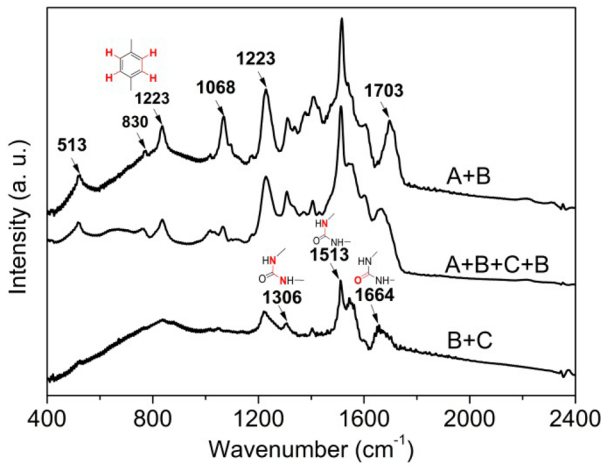

Figure 1. FTIR spectra of the MLD films prepared using $Zn(Et)_2$ (A), PPDI (B), and EDA (C) as molecular precursors with different reaction sequence at 100 °C.

of urea and zinc amidate and the formation of Zn-hybrid film using the four-step ABCB reaction sequence. To confirm this, MLD processes with $Zn(Et)_2$ and PPDI (A + B) as precursors and with PPDI and EDA (B + C) as precursors were also conducted. For B + C MLD film (Polyurea), three bands at 1664 (C═O stretching vibration), 1513 (C−N stretching), and 1306 (N−C−N stretching) cm^{-1} are characteristic of a polyurea linkage.[35] The A+B MLD film shows three different peaks at 1703, 1068, and 513 cm^{-1}, corresponding to N,O-chelating amidate moieties bonded with Zn atom.[34] The peak at 1068 cm^{-1} is also observed in the FTIR of ABCB MLD film. Besides, all MLD films containing PPDI (B) monomers have the peaks at 1223 cm^{-1} (in-plane bending of C═C−H in Ph ring), and 830 cm^{-1} (out-plane bending of C═C−H in Ph ring). Typical bands of the B + C and A + B MLD films are also present in the spectrum of ABCB MLD film. This reveals the covalent bonding of urea with zinc amidate in the Zn-hybrid film. For the XPS spectrum of ABCB MLD film, all the Zn 2p, N 1s and O 1s spectra can be fit to a single peak, indicating a single form for each element. However, from the reaction (Scheme 1), there should be three distinct nitrogen atoms in the ABCB MLD film: the amide nitrogen bonded to the Zn ion, the amide nitrogen bonded to the alkyl carbon, and the amide nitrogen bonded to the aryl carbon. This indicates that these nitrogen atoms are too electronically similar to be resolved by XPS. Similar results were observed for the case of MLD polyurea films[33] and Polythiourea.[37] The C 1s spectrum of ABCB MLD film contains three distinct feature peaks, attributed to the aromatic carbon, alkyl carbon (C−N), and carbonyl carbons (C═O), respectively.[33]

The Zn-hybrid MLD film was deposited onto the Cu precursors supported on CNTs to prepare the Cu−Zn-MLD catalysts. After 80 cycles of MLD, a uniform Zn-hybrid film of 40 nm thickness is successfully coated on the surface of the sample (Figure 2A), which is clearly visible from its brighter contrast. The interlayer with a darker contrast located between the Zn-hybrid MLD film and CNTs corresponds to the copper precursors. Figure 2B shows the typical TEM image of the calcinated Cu−Zn120MLD sample, which exhibits a uniform dispersion of CuO and ZnO NPs on the CNTs. After reduction, the NPs on the surface of CNTs are closely contacted with each

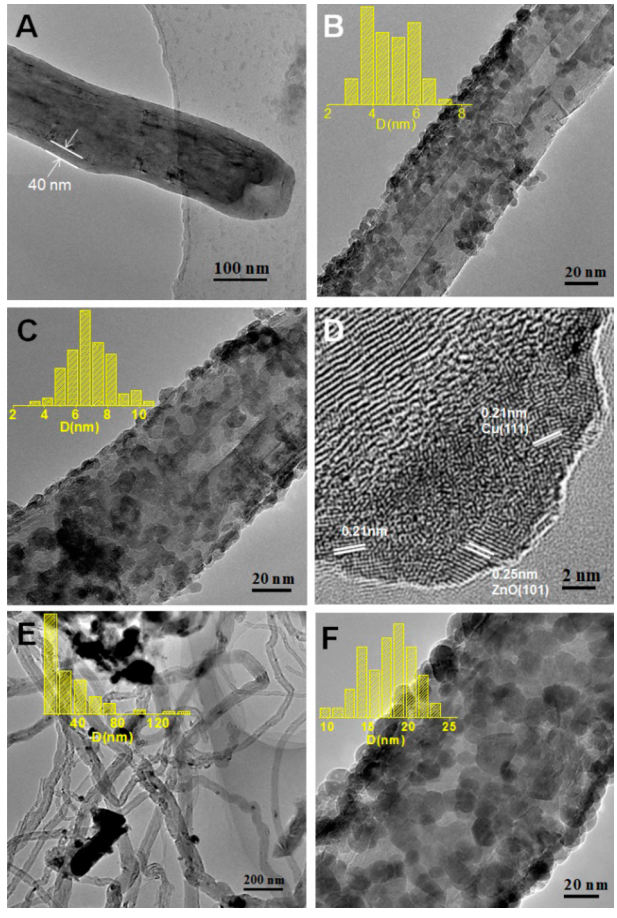

Figure 2. (A) Cu−Zn80MLD before calcination; (B) Cu−Zn120MLD after calcination at 300 °C in air; (C) Cu−Zn120MLD reduced at 300 °C in H_2/N_2; (D) HRTEM of reduced Cu−Zn120MLD; (E) Reduced Cu/CNTs; (F) Reduced Cu−Zn120ALD.

DOI: 10.1021/acscatal.5b01266
ACS Catal. 2015, 5, 5567−5573

other (Figure 2C). Figure 2B and 2C reveal that the average particle size of the NPs on CNTs is around 6 nm. HRTEM was used to reveal the microstructure of Cu-ZnO interface. The interplanar spacing of 0.21 and 0.25 nm (Figure 2D) matches well with the (111) plane of Cu^0 and (101) plane of ZnO, respectively. The Cu^0 NPs are interacted with ZnO NPs. In contrast, the Cu^0 NPs of reduced Cu/CNTs catalyst have a broad size distribution ranging from 2 to 300 nm (Figure 2E). Therefore, it can be inferred that the ZnO NPs interacting with CuO NPs can prevent the agglomeration of Cu^0 NPs and promote the generation of Cu-ZnO interface during reduction. For comparison, copper catalysts modified by direct ALD of ZnO were also prepared and designated as Cu−Zn-ALD. Figure 2F shows that ZnO particles with a diameter of 11−18 nm are attached on the surface of the reduced Cu−Zn120ALD catalyst.

XRD patterns and TG curves of the samples are illustrated in Figure 3 and Figure S3. The Cu precursors on the CNTs before MLD are mixtures of $Cu_2(OH)_3NO_3$, $CuNH_3(NO_3)_2$ and $Cu(OH)_2$, which are mainly converted into $Cu(EDA)_2(NO_3)_2$ after Zn-hybrid MLD process (Figure 3A). This indicates that the Zn-hybrid MLD film interacts with the copper precursors through copper coordination with EDA. TG analysis (Figure 3C) shows that the decomposition temperatures of the copper precursors and Zn-hybrid MLD films are below 350 °C in air. After calcination in air at 300 °C, copper precursors and Zn MLD films are converted into CuO and ZnO NPs, respectively (Figure S3). XRD analysis reveals that all the CuO NPs are further converted into Cu^0 after reduction (Figure 3B). The XRD peak of the Cu(111) around 43.2° for the reduced Cu/CNTs is significantly narrower than those in other reduced Cu−Zn-MLD catalysts. Crystallite size of Cu NPs for these samples was calculated by using the Scherrer equation based on the fwhm of the Cu(111) diffraction peak (Figure 3B). Crystallite size of Cu NPs follows the order: Cu/CNTs (11 nm) > Cu−Zn40MLD (6 nm) > Cu−Zn80MLD (5 nm) > Cu−Zn120MLD (4 nm), indicating that the Zn MLD film prevents the agglomeration of Cu^0 NPs during preparation process. This is consistent with the TEM results. The interaction between ZnO and Cu may also result in the line broadening of the XRD peaks. The lattice constant of Cu^0 is determined from the XRD peak position of the Cu(111). However, the lattice constant of Cu^0 for Cu−Zn-MLD is similar to that of Cu/CNTs, indicating that the ZnO species is not dissolved into the Cu particles to form a Cu−Zn alloy.[16] Figure 3B(5) reveals the formation of larger ZnO particles for the Cu−Zn120ALD from the obvious sharp peaks. The peaks of Cu^0 are invisible in the reduced Cu−Zn120ALD catalyst due to the overcoating of ALD ZnO.

XPS and AES analyses of the reduced catalysts were carried out to obtain a detailed chemical environment of the Cu-ZnO interface. The absence of "shakeup" peaks in Cu 2p spectra (Figure 4A, Figure S5A) indicates that the Cu^{2+} is completely reduced to metallic copper (Cu^0) and/or Cu^{1+} for the reduced Cu−Zn-MLD, Cu/CNTs, and Cu−Zn-ALD catalysts.[29] Cu^0 and Cu^+ can be distinguished from the AES spectra (Figure 4B). For the reduced Cu/CNTs catalyst, only two AES peaks are observed at 918.8 and 916.7 eV, attributing to Cu^0 and Cu^+, respectively.[3,29,38] However, a new AES peak appears at 918.3 eV for the Cu−Zn-MLD catalysts in addition to the peaks observed in the Cu/CNTs catalyst. Moreover, the intensity of the peak at 918.3 eV increases with the increase of Zn MLD cycle number from 40 to 120, while the intensity of the peak at 918.8 eV is dramatically decreased. The peak at 918.3 eV is due to the Cu^0 species which have interaction with the ZnO, labeled as

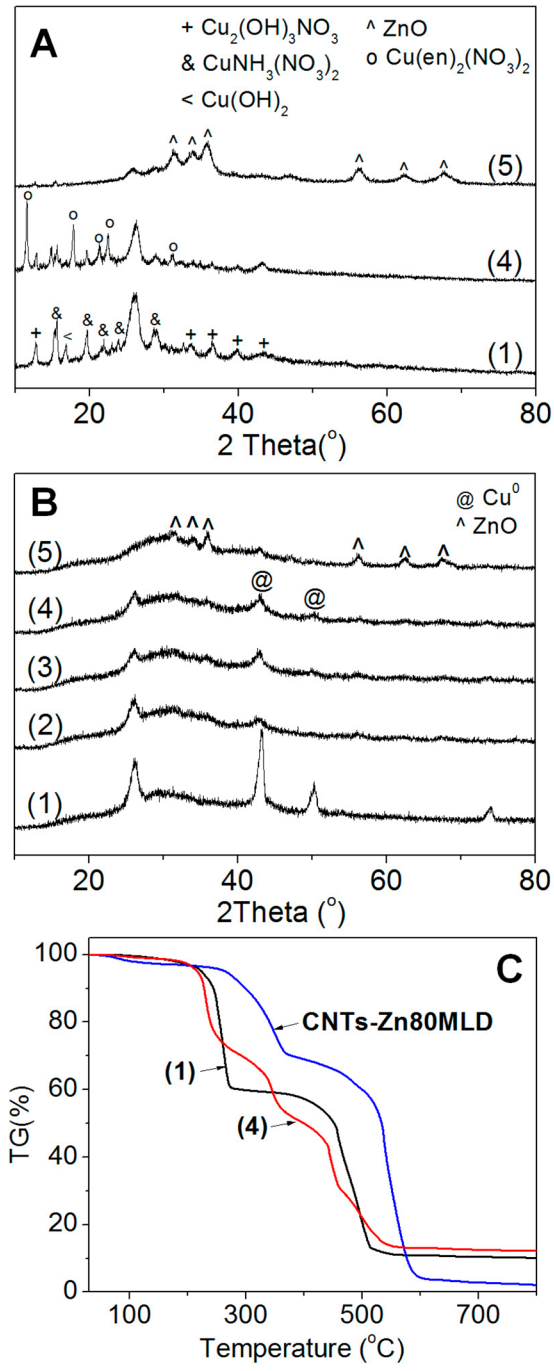

Figure 3. (A) XRD patterns of the samples before calcination; (B) XRD patterns of the samples after reduction in H_2/N_2 at 300 °C; (C) TG curves of the samples before calcination. Samples: (1) Cu/CNTs; (2) Cu−Zn40MLD; (3) Cu−Zn80MLD; (4) Cu−Zn120MLD; (5) Cu−Zn120ALD.

Cu^0Zn.[38] No peak at 919.1 eV is observed, suggesting the absence of two-dimensional epitaxial Cu^0 monolayer on the surface of ZnO NPs.[38,39] For the Cu−Zn160MLD catalyst, the AES peak at 918.8 eV disappears, suggesting most of the Cu^0 species are converted into Cu^0Zn species. In order to understand the electrical density change of the Cu^0Zn species, the modified Auger parameter [$\alpha' = KE(Cu_{LMM}) + BE(Cu\ 2p_{3/2})$] was introduced.[40] The α' for Cu^0Zn (KE = 918.3 eV) is 1850.8 eV, which is lower than that of Cu^0 (α' = 1851.3 eV). This indicates the electron density increases on Cu^0Zn compared with that on

DOI: 10.1021/acscatal.5b01266
ACS Catal. 2015, 5, 5567−5573

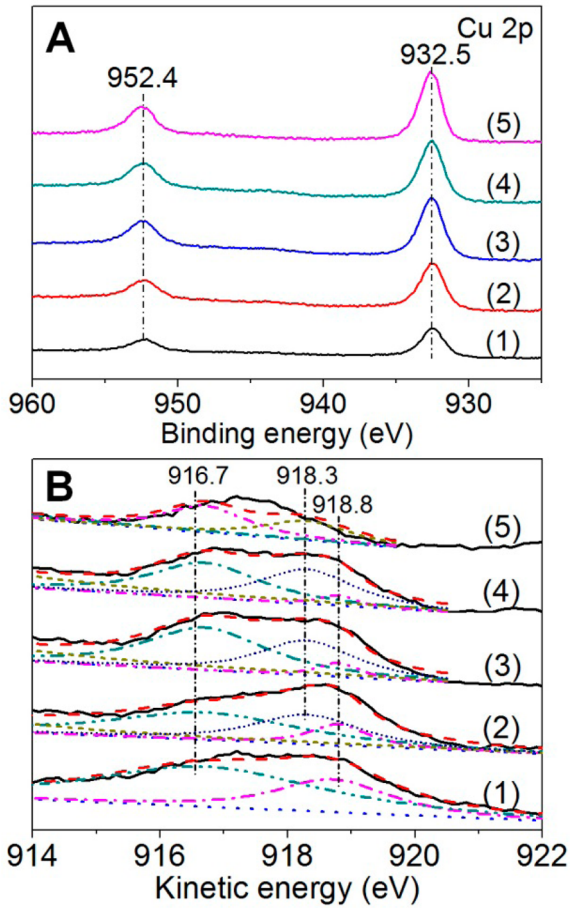

Figure 4. XPS and AES of reduced samples. (A) XPS of Cu 2p; (B) AES of Cu_{LMM} Samples: (1) Cu/CNTs; (2) Cu−Zn40MLD; (3) Cu−Zn80MLD; (4) Cu−Zn120MLD; (5) Cu−Zn160MLD.

pure Cu^0.[38,39] Electron transfer from ZnO to Cu is further revealed from the XPS of O 1s. Figure S4B shows that two oxygen species, the hydroxyl group on the ZnO surface (531.6 eV) and the crystal lattice oxygen in ZnO (530.7 eV),[15,40] are produced on the reduced Cu−Zn-MLD catalyst due to the loading of ZnO NPs. The binding energy (BE) of The lattice oxygen in Cu−Zn-MLD is higher than that on pure ZnO (530.2 ± 0.2 eV[17,41]), suggesting the electron transfer from ZnO NPs to Cu NPs at the Cu-ZnO interface.[15] Because the lattice oxygen is responsible for the electoral transfer between ZnO and Cu NPs, the content of the lattice oxygen species is also correlated with the content of Cu-ZnO interface sites. Therefore, the ratio of the lattice oxygen in ZnO is increased with the increase of Zn MLD cycle number, indicating the increase of Cu-ZnO interface sites.

Previous studies reveal that the reduction process of Cu−Zn-based catalysts usually results in the formation of Cu−Zn alloy.[4,16] However, on the surface of reduced Cu−Zn-MLD (Figure S4C), all the BE of Zn $2p_{3/2}$ is located at 1022.1 eV, which is higher than that that of ZnO bulk (1021.7 eV)[40] and similar to partially reduced ZnO_x on the surface of Cu(111) (1021.9 eV).[42] AES of Zn LMM is more sensitive than the Zn 2p spectra to the chemical environment. Only two AES peaks are observed at 991.2 and 988.1 eV (Figure S4D). No peak at 992.4 eV is observed in the AES of Zn LMM, indicating that no Zn metal or alloy but ZnO or ZnO_x is present on the surface of reduced Cu−Zn-MLD.[38,39,43,44] The α' [α' = BE(Zn $2p_{3/2}$) + KE(Zn LMM)] for the two Zn species were 2013.3 and 2010.2 eV, attributing to ZnO_x and pure ZnO, respectively.[40,43]

It was reported that the formation of metal-oxides interface by ALD or MLD is realized at the expense of metal surface sites.[21,22,27,28] However, the Zn MLD process here does not result in loss of copper surface sites. Based on the XPS result (Table S2), the surface Cu/Zn ratio of Cu−Zn-MLD is calculated to be 0.3. Interestingly, such ratio reduces slowly along with the increase of MLD cycle number. In contrast to this, the Cu/Zn ratio of Cu−Zn-ALD drop significantly with the increase of Zn ALD cycle number due to the ZnO overcoating.

The hydrogenation of LA was carried out to evaluate the performance of Cu/CNTs, Cu−Zn-MLD and Cu−Zn-ALD catalysts. It is revealed that the Cu−Zn-MLD catalysts have much better performance for the synthesis of GVL than that of Cu/CNTs (Figure 5). The catalytic activity of Cu−Zn-MLD raise

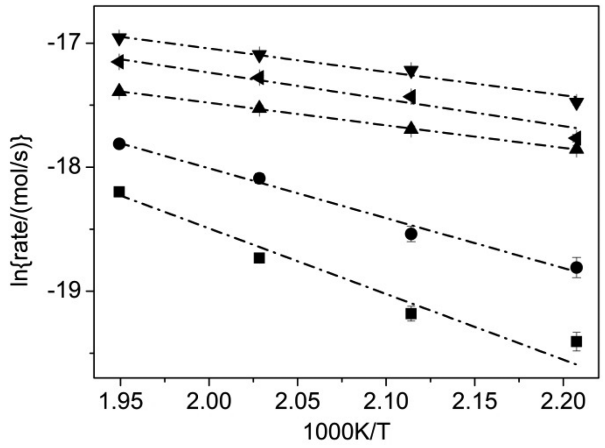

Figure 5. Arrhenius plot for GVL synthesis from LA hydrogenation on Cu/CNTs (■), Cu−Zn40MLD (●), Cu−Zn80MLD (▲), Cu−Zn120MLD (▼), and Cu−Zn160MLD (◀). These values are obtained at the steady-state measured at 180, 200, 220, and 240 °C, respectively.

first but slightly reduced by increasing the MLD cycle number from 40 to 120 and then to 160. In contrast, the yield of GVL on Cu−Zn-ALD is not substantially raised with the increase of Zn ALD cycle number (Table S3). The apparent activation energy (E_a) of GVL formation was calculated according to the Arrhenius equation ($k = Ae^{(-E_a/RT)}$) (Table S3). The E_a of GVL formation on Cu/CNTs is 38.9 ± 5.5 kJ/mol, which is comparable with previous values ranging from 33 to 59 kJ/mol over Cu-based catalyst in C═O bond hydrogenation of CO (33.6−41.8 kJ/mol),[45] CO_2 (58.8 kJ/mol),[46] and acetophenone (54.9 kJ/mol).[47] However, the E_a of GVL formation is dramatically decreased on the Cu−Zn80MLD (15.1 ± 0.3 kJ/mol), Cu−Zn120MLD (15.7 ± 1.6 kJ/mol), and Cu−Zn160MLD (17.9 ± 2.1 kJ/mol), suggesting the generation of new surface active sites with high catalytic efficiency due to the Cu-ZnO interaction.

Generally, high copper surface area is advantageous to the hydrogenation activity of Cu catalyst.[48] Table S3 shows the metallic copper surface areas (S_{Cu}) of the reduced catalysts and the turnover frequency (TOF) of GVL. The S_{Cu} of Cu/CNTs is lower than that of Cu−Zn-MLD but higher than that of Cu−Zn-ALD. Moreover, the S_{Cu} of Cu−Zn-MLD slightly increases with the Zn MLD cycle number. Therefore, Zn MLD results in the generation of more Cu^0 sites, and Zn ALD leads to the decrease of Cu^0 sites. This accounts for the enhanced GVL yield on Cu−Zn-MLD as well as the low activity of Cu−Zn-ALD. All TOF

DOI: 10.1021/acscatal.5b01266
ACS Catal. 2015, 5, 5567−5573

values of Cu−Zn-MLD or Cu−Zn-ALD are higher than those of Cu/CNTs (4.0 h^{-1}) and commercial Cu−Zn−Al catalyst (MWC-612, 3.0 h^{-1}). The Cu−Zn120MLD turns to be most efficient catalyst with a TOF value of 11.3 h^{-1}, which is nearly 3 times higher than that of Cu/CNTs. This reveals that the formation of additional surface microstructure enhances the activity of Cu NPs due to ZnO interaction.[4,49]

AES analysis of the reduced catalysts indicates that the content of new Cu^0Zn species increases with the increase of MLD cycle number. On the contrary, the amount of Cu^0 and Cu^+ reduce with the increase of Zn MLD cycle number. This can be ascribed to the interaction between Cu and ZnO NPs. To further gain insight into the effect of Cu valence state in the LA hydrogenation to GVL, the TOF of GVL as a function of ratio of different copper valences was examined. Figure 6A shows that

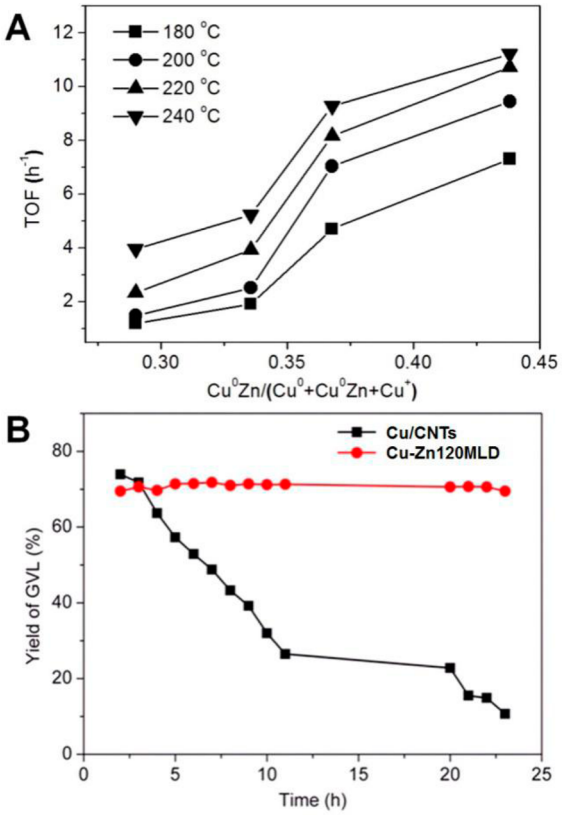

Figure 6. (A) Correlation of the TOF of GVL yield with $Cu^0Zn/(Cu^0 + Cu^0Zn + Cu^+)$; (B) The stability of the catalysts in the hydrogenation of LA (240 °C, 1 MPa, H_2/N_2 = 0.5).

TOF increases with the $Cu^0Zn/(Cu^0 + Cu^0Zn + Cu^+)$ ratio at different reaction temperatures, suggesting that the catalytic activity mainly depends on the number of Cu^0Zn sites. In contrast, the ratio of $Cu^0/(Cu^0 + Cu^0Zn + Cu^+)$ and $Cu^+/(Cu^0 + Cu^0Zn + Cu^+)$ decrease with the increase of Zn MLD cycle number (Figure S6). Since the TOF is not perfectly lineally increased with the $Cu^0Zn/(Cu^0 + Cu^0Zn + Cu^+)$ ratio, it would be reasonable to assume the subsidiary of Cu^0 and Cu^+ in the hydrogenation of LA over the Cu−Zn-MLD catalyst.

In the vapor-phase LA hydrogenation, surface adsorption and activation of reactants (H_2 and LA) and intermediates are vital catalytic steps. Different mechanisms have been proposed in previous works to interpret the C═O hydrogenation behaviors over the Cu-based catalysts. Chen and co-workers have demonstrated that a modest $Cu^0/(Cu^0 + Cu^+)$ ratio on the surface leads to the optimal TOF in ester hydrogenation, and Cu^0 is the primary active site, while Cu^+ may facilitate the conversion of intermediates.[3] Our results indicate that Cu^0Zn is the key copper species to induce high activity for LA hydrogenation over Cu−Zn-MLD catalyst, and that Cu^+ species decreases with the increase of Zn MLD cycle number. Although Cu^+ may facilitate the conversion of intermediates, it is not the key catalytic site. We have found that the E_a of GVL formation is obviously reduced over Cu−Zn80MLD, Cu−Zn120MLD and Cu−Zn160MLD in comparison with Cu/CNTs. XPS and AES analyses reveal that the Zn species is partially reduced to ZnO_x by interacting with Cu, owing to the Cu−Zn electron transfer at the interface of Cu-ZnO. In CO hydrogenation, in situ XPS and theoretical simulation indicated that $Zn^{\delta+}$ species at Cu steps/defects result in the increasing of binding strength of intermediate (HC═O*, H_2C═O*) and decreasing of reaction barriers.[4] This is consistent with our results, indicating that the Cu-ZnO interface site (Cu^0Zn) has special activity and low energy barriers in hydrogenation of LA.

Figure 6B displays the comparison of catalytic activity as a function of reaction time for the Cu−Zn120MLD catalyst and the Cu/CNTs catalyst. The yield of GVL is dramatically decreased from 73% to 10% over the Cu/CNTs catalyst. However, there is no obvious change in the yield of GVL for the Cu-Zn120MLD catalyst. Yue and co-workers reported that higher $Cu^0/(Cu^0 + Cu^+)$ ratio (0.27) on the Cu@PSNT-in leads to an enhanced stability.[7] Analogously, the interaction between the Cu NPs and ZnO NPs and increase of $Cu^0Zn/(Cu^0 + Cu^0Zn + Cu^+)$ ratio also induce the high stability of the Cu−Zn120MLD catalyst by suppressing the sintering of Cu NPs. This MLD method has also been used to deposit Zn MLD film onto a Cu−based catalyst, which was prepared by a direct precipitation method using sodium hydroxide as precipitant (Cu-Pre-Zn120MLD). Similarly, the catalytic activity and TOF of the Cu-based catalyst were dramatically increased in LA hydrogenation after Zn MLD modification (Table S3).

4. CONCLUSIONS

In conclusion, we have demonstrated a new approach to tailoring the Cu-ZnO interface by depositing Zn-hybrid film with controlled thickness by MLD on Cu precursors supported on CNTs. Cu NPs are uniformly mixed with small ZnO NPs to form more Cu-ZnO interface sites, which have intrinsic catalytic activity and stability in LA hydrogenation by reducing the apparent activation energy. In contrast, the Cu catalysts modified with ALD ZnO result in the covering of the Cu surface sites and low yield of GVL. The tailoring of Cu-ZnO interface of Cu−Zn-MLD catalysts can pave the way for other similar C═O hydrogenation processes, such as the hydrogenation of furfural,[22] CO, CO_2[4] and dimethyl maleate.[7] Production of new Cu^0Zn site by Cu-ZnO interaction via MLD could help us to better understand the nature of the copper active sites and the synergy of metal and metal oxide interface in the C═O hydrogenation.

■ ASSOCIATED CONTENT

Supporting Information

The Supporting Information is available free of charge on the ACS Publications website at DOI: 10.1021/acscatal.5b01266.

TEM images of Cu−Zn120MLD and Cu−Zn120ALD catalysts after reduction; XRD of the samples after calcination in air at 300 °C; XPS spectra of Zn-hybrid

DOI: 10.1021/acscatal.5b01266
ACS Catal. 2015, 5, 5567−5573

films; XPS and AES analysis of reduced Cu−Zn-MLD and Cu−Zn-ALD catalysts; Correlation of the TOF of GVL yield with $Cu^0/(Cu^0 + Cu^0Zn + Cu^+)$ and $Cu^+/(Cu^0 + Cu^0Zn + Cu^+)$ for the Cu/CNTs and Cu−Zn-MLD catalysts; Surface composition analysis of the reduced catalysts, physicochemical properties of the catalysts, and their catalytic performance for LA hydrogenation to GVL; Uncertainties on experimental data points of Arrhenius plot for LA hydrogenation (PDF)

AUTHOR INFORMATION

Corresponding Author

*E-mail: qinyong@sxicc.ac.cn.

Notes

The authors declare no competing financial interest.

ACKNOWLEDGMENTS

We appreciate the financial support from the National Natural Science Funds of China (21403271, 21173248, and 21376256), the Hundred Talents Program of the Chinese Academy of Sciences, the Hundred Talents Program of Shanxi Province, and the Projects of the State Key Laboratory of Coal Conversion of China (2014BWZ004).

REFERENCES

(1) Deng, L.; Li, J.; Lai, D.-M.; Fu, Y.; Guo, Q.-X. *Angew. Chem., Int. Ed.* **2009**, *48*, 6529−6532.
(2) Lange, J.-P.; van der Heide, E.; van Buijtenen, J.; Price, R. *ChemSusChem* **2012**, *5*, 150−166.
(3) Gong, J.; Yue, H.; Zhao, Y.; Zhao, S.; Zhao, L.; Lv, J.; Wang, S.; Ma, X. *J. Am. Chem. Soc.* **2012**, *134*, 13922−13925.
(4) Behrens, M.; Studt, F.; Kasatkin, I.; Kühl, S.; Hävecker, M.; Abild-Pedersen, F.; Zander, S.; Girgsdies, F.; Kurr, P.; Kniep, B.-L.; Tovar, M.; Fischer, R. W.; Nørskov, J. K.; Schlögl, R. *Science* **2012**, *336*, 893−897.
(5) Hengne, A. M.; Rode, C. V. *Green Chem.* **2012**, *14*, 1064−1072.
(6) Besson, M.; Gallezot, P.; Pinel, C. *Chem. Rev.* **2014**, *114*, 1827−1870.
(7) Yue, H.; Zhao, Y.; Zhao, S.; Wang, B.; Ma, X.; Gong, J. *Nat. Commun.* **2013**, *4*, 2339.
(8) Farmer, J. A.; Campbell, C. T. *Science* **2010**, *329*, 933−936.
(9) Yuan, J.; Li, S.-S.; Yu, L.; Liu, Y.-M.; Cao, Y.; He, H.; Fan, K. *Energy Environ. Sci.* **2013**, *6*, 3308−3313.
(10) Zhu, S.; Gao, X.; Zhu, Y.; Zhu, Y.; Zheng, H.; Li, Y. *J. Catal.* **2013**, *303*, 70−79.
(11) Chen, L.-F.; Guo, P.-J.; Qiao, M.-H.; Yan, S.-R.; Li, H.-X.; Shen, W.; Xu, H.-L.; Fan, K.-N. *J. Catal.* **2008**, *257*, 172−180.
(12) Behrens, M. *J. Catal.* **2009**, *267*, 24−29.
(13) Liu, X.-M.; Lu, G. Q.; Yan, Z.-F.; Beltramini, J. *Ind. Eng. Chem. Res.* **2003**, *42*, 6518−6530.
(14) Nakamura, J.; Uchijima, T.; Kanai, Y.; Fujitani, T. *Catal. Today* **1996**, *28*, 223−230.
(15) Liao, F.; Huang, Y.; Ge, J.; Zheng, W.; Tedsree, K.; Collier, P.; Hong, X.; Tsang, S. C. *Angew. Chem., Int. Ed.* **2011**, *50*, 2162−2165.
(16) Le Valant, A.; Comminges, C.; Tisseraud, C.; Canaff, C.; Pinard, L.; Pouilloux, Y. *J. Catal.* **2015**, *324*, 41−49.
(17) Simon, Q.; Barreca, D.; Gasparotto, A.; Maccato, C.; Montini, T.; Gombac, V.; Fornasiero, P.; Lebedev, O. I.; Turner, S.; Van Tendeloo, G. *J. Mater. Chem.* **2012**, *22*, 11739−11747.
(18) Kniep, B. L.; Ressler, T.; Rabis, A.; Girgsdies, F.; Baenitz, M.; Steglich, F.; Schlögl, R. *Angew. Chem., Int. Ed.* **2004**, *43*, 112−115.
(19) Simon, Q.; Barreca, D.; Gasparotto, A.; Maccato, C.; Tondello, E.; Sada, C.; Comini, E.; Sberveglieri, G.; Banerjee, M.; Xu, K.; Devi, A.; Fischer, R. A. *ChemPhysChem* **2012**, *13*, 2342−2348.
(20) George, S. M. *Chem. Rev.* **2010**, *110*, 111−131.
(21) O'Neill, B. J.; Jackson, D. H. K.; Crisci, A. J.; Farberow, C. A.; Shi, F.; Alba-Rubio, A. C.; Lu, J.; Dietrich, P. J.; Gu, X.; Marshall, C. L.; Stair, P. C.; Elam, J. W.; Miller, J. T.; Ribeiro, F. H.; Voyles, P. M.; Greeley, J.; Mavrikakis, M.; Scott, S. L.; Kuech, T. F.; Dumesic, J. A. *Angew. Chem., Int. Ed.* **2013**, *52*, 13808−13812.
(22) Zhang, H.; Lei, Y.; Kropf, A. J.; Zhang, G.; Elam, J. W.; Miller, J. T.; Sollberger, F.; Ribeiro, F.; Akatay, M. C.; Stach, E. A.; Dumesic, J. A.; Marshall, C. L. *J. Catal.* **2014**, *317*, 284−292.
(23) Peng, Q.; Gong, B.; VanGundy, R. M.; Parsons, G. N. *Chem. Mater.* **2009**, *21*, 820−830.
(24) Gong, B.; Peng, Q.; Parsons, G. N. *J. Phys. Chem. B* **2011**, *115*, 5930−5938.
(25) Abdulagatov, A. I.; Hall, R. A.; Sutherland, J. L.; Lee, B. H.; Cavanagh, A. S.; George, S. M. *Chem. Mater.* **2012**, *24*, 2854−2863.
(26) Liang, X.; Yu, M.; Li, J.; Jiang, Y.-B.; Weimer, A. W. *Chem. Commun.* **2009**, 7140−7142.
(27) Liang, X.; Li, J.; Yu, M.; McMurray, C. N.; Falconer, J. L.; Weimer, A. W. *ACS Catal.* **2011**, *1*, 1162−1165.
(28) Gould, T. D.; Izar, A.; Weimer, A. W.; Falconer, J. L.; Medlin, J. W. *ACS Catal.* **2014**, *4*, 2714−2717.
(29) Zhang, B.; Zhu, Y.; Ding, G.; Zheng, H.; Li, Y. *Appl. Catal., A* **2012**, *443*−*444*, 191−201.
(30) Bond, G. C.; Namijo, S. N. *J. Catal.* **1989**, *118*, 507−510.
(31) Vandergrift, C. J. G.; Wielers, A. F. H.; Joghi, B. P. J.; Vanbeijnum, J.; Deboer, M.; Versluijshelder, M.; Geus, J. W. *J. Catal.* **1991**, *131*, 178−189.
(32) Dandekar, A.; Vannice, M. A. *J. Catal.* **1998**, *178*, 621−639.
(33) Chen, Y.; Zhang, B.; Gao, Z.; Chen, C.; Zhao, S.; Qin, Y. *Carbon* **2015**, *82*, 470−478.
(34) Schmidt, S.; Schäper, R.; Schulz, S.; Bläser, D.; Wölper, C. *Organometallics* **2011**, *30*, 1073−1078.
(35) Loscutoff, P. W.; Zhou, H.; Clendenning, S. B.; Bent, S. F. *ACS Nano* **2010**, *4*, 331−341.
(36) Chen, C.; Li, P.; Wang, G.; Yu, Y.; Duan, F.; Chen, C.; Song, W.; Qin, Y.; Knez, M. *Angew. Chem., Int. Ed.* **2013**, *52*, 9196−9200.
(37) Loscutoff, P. W.; Lee, H.-B.-R.; Bent, S. F. *Chem. Mater.* **2010**, *22*, 5563−5569.
(38) Okamoto, Y.; Fukino, K.; Imanaka, T.; Teranishi, S. *J. Phys. Chem.* **1983**, *87*, 3747−3754.
(39) Velu, S.; Suzuki, K.; Vijayaraj, M.; Barman, S.; Gopinath, C. S. *Appl. Catal., B* **2005**, *55*, 287−299.
(40) Simon, Q.; Barreca, D.; Gasparotto, A. *Surf. Sci. Spectra* **2010**, *17*, 93−101.
(41) Feng, W.; Wan, A. S.; Garfunkel, E. *J. Phys. Chem. C* **2013**, *117*, 9852−9863.
(42) Sano, M.; Adaniya, T.; Fujitani, T.; Nakamura, J. *Surf. Sci.* **2002**, *514*, 261−266.
(43) Wehner, P. S.; Mercer, P. N.; Apai, G. *J. Catal.* **1983**, *84*, 244−247.
(44) Wagner, C. D.; Biloen, P. *Surf. Sci.* **1973**, *35*, 82−95.
(45) Karelovic, A.; Bargibant, A.; Fernández, C.; Ruiz, P. *Catal. Today* **2012**, *197*, 109−118.
(46) Nakano, H.; Nakamura, I.; Fujitani, T.; Nakamura, J. *J. Phys. Chem. B* **2001**, *105*, 1355−1365.
(47) Bertero, N. M.; Apesteguía, C. R.; Marchi, A. J. *Appl. Catal., A* **2008**, *349*, 100−109.
(48) Zheng, X.; Lin, H.; Zheng, J.; Duan, X.; Yuan, Y. *ACS Catal.* **2013**, *3*, 2738−2749.
(49) Ressler, T.; Kniep, B. L.; Kasatkin, I.; Schlögl, R. *Angew. Chem., Int. Ed.* **2005**, *44*, 4704−4707.

DOI: 10.1021/acscatal.5b01266
ACS Catal. 2015, 5, 5567−5573